

Subharmonics and superharmonics of the weak field in a driven two-level quantum system: Vibrational resonance enhancement

Prasun Sarkar, Shibashis Paul, and Deb Shankar Ray ^{*}*Indian Association for the Cultivation of Science, Jadavpur, Kolkata-700032, India*

(Received 16 April 2021; accepted 9 June 2021; published 2 July 2021)

We consider a quantum two-level system in bichromatic classical time-periodic fields, the frequency of one of which far exceeds that of the other. Based on systematic separation of timescales and averaging over the fast motion a reduced quantum dynamics in the form of a nonlinear forced Mathieu equation is derived to identify the stable oscillatory resonance zones intercepted by unstable zones in the frequency-amplitude plot. We show how this forcing of the dressed two-level system may generate the subharmonics and superharmonics of the weak field in the stable region, which can be amplified by optimization of the strength of the high frequency field. We have carried out detailed numerical simulations of the driven quantum dynamics to corroborate the theoretical analysis.

DOI: [10.1103/PhysRevE.104.014202](https://doi.org/10.1103/PhysRevE.104.014202)

I. INTRODUCTION

The dynamic response of a nonlinear system to one or more deterministic or stochastic driving fields is often characterized by resonances when one of the system parameters is varied. A typical such resonance phenomenon was discovered in the early 1980s of the past century when the response of a bistable system to a weak signal field was shown to be amplified by varying the strength of the noise applied on the system [1]. This noise-induced effect, the stochastic resonance [2–5], and several of its variants, e.g., resonant activation [6–8], coherence resonance [9,10], noise-induced transition of stability [11,12], and noise-induced pattern formation and wave propagation [13–16] have significantly modified our understanding of the counterintuitive, constructive positive role of noise in a wide variety of phenomena associated with climate change [1], bistable circuits [3], lasers [4], chemical reactions [17], synchronization [18], and information processing [19] to name a few. An interesting deterministic variant of stochastic resonance is vibrational resonance, discovered in early 2000 by Landa and McClintock [20] in a numerical exploration of a bistable system where the noise was replaced by a high-frequency time-varying field. This was followed further by theoretical [21–24] and experimental [25–28] investigations and a plethora of new development that includes entropic [29], logical [30], anti- [31] and ghost [32], nonlinear [27,33,34] vibrational resonance and vibrational ratchet [35] along with experimental applications in material processing, image processing, fault detection, logic gate operations, and energy harvesting. We refer to [36] for a state-of-the-art review of this field.

The overwhelming majority of the studies on vibrational resonance concern classical nonlinear dynamical systems

in which two periodic fields are simultaneously applied as additive forcing [20–24]. The frequency of the fast time-varying field far exceeds that of the other. Vibrational resonance is observed by examining the response of the system to the weak field by optimizing the strength of the high frequency field. However, when one of the fields appears as a multiplicative forcing, one encounters a parametrically driven forced system. Nonlinear resonances [37] in these systems are often accompanied by instability and multistability. Our focus in this paper is to explore this nonlinear resonance-induced instability and oscillations in a quantum system [38,39]. In what follows, we consider a two-level quantum system driven by bichromatic fields described by lossless Bloch equations [40–42] which govern the dynamics of quantum mechanical average values of three Pauli spin operators, with two representing the polarization variables while the third one refers to the population inversion variable. Bloch equations have been widely employed in quantum optics and magnetic resonance spectroscopy and a wide variety of solutions [43–46] have been known over nearly half a century. In the present context of Bloch equations, we show that the use of normalization of quantum probability and averaging over the fast motion results in an effective quantum dynamics of the dressed two-level system in the form of a forced nonlinear Mathieu equation [47–49]. The object of the present paper is (i) to explore the subharmonic and superharmonic resonant response of the dressed two-level system to the weak periodic field, (ii) to understand the resonance zones and oscillations intercepted by instability zones inside Arnold's tongue in the weak field amplitude-frequency plot, and (iii) to probe how these subharmonic and superharmonic responses can be enhanced by optimization of the strength and frequency of the fast time-varying field. We use a multiple timescale perturbation method for removing the secular divergences arising out of the resonance condition and figure out the regular oscillatory domain and instability

^{*}Corresponding author: pcdsr@iacs.res.in

zones in the parametric space. Our theoretical analysis is corroborated by full numerical simulation of the Bloch dynamics.

The rest of the paper is organized as follows. In Sec. II, we introduce the Bloch equations describing the dynamics of a two-level system driven by two classical time-periodic fields with widely differing frequencies. The equations are cast into a form to allow implementation of the methods of multiple timescales to arrive at a nonlinear forced Mathieu equation. The perturbative theory is used to derive the solvability condition for each of the resonance cases, which allows us to figure out the stability zones in the amplitude-frequency plot in Sec. III. In Sec. IV, we perform numerical simulation of Bloch equations for sub- and superharmonic resonance corresponding to our analytical scheme to demonstrate the resonance oscillations and instability zones and vibrational enhancement of resonance. The paper is concluded in Sec. V.

II. BLOCH EQUATIONS FOR A TWO-LEVEL QUANTUM SYSTEM DRIVEN BY TWO CLASSICAL FIELDS

A. General considerations

We consider a quantum two-level system interacting with bichromatic classical electromagnetic fields $c \cos(\omega t)$ and $G \cos(\Omega t)$, where c and G are the amplitudes and ω and Ω represent the frequencies of the two fields, respectively. We use Bloch equations [42] to study the dynamics of the system as follows:

$$\dot{x} = -\omega_0 y(t), \quad (2.1)$$

$$\dot{y} = \omega_0 x(t) + \chi f(t) z(t), \quad (2.2)$$

$$\dot{z} = -\chi f(t) y(t), \quad (2.3)$$

where x , y , and z represent the quantum mechanical mean values of the corresponding Pauli spin operators; x and y are the polarization variables and z denotes to the population difference between the two levels. χ refers to the scaled transition dipole moment for the two levels, defined as $\chi = 2d/\hbar$; \hbar is the reduced Planck constant (defined as $h/2\pi$). Here the term $f(t)$ is given as follows:

$$f(t) = f_0 + c \cos(\omega t) + g \cos(\Omega t), \quad (2.4)$$

where f_0 is a constant field and the system is perturbed simultaneously by a high frequency field ($g \cos \Omega t$), as well as by a low frequency field ($c \cos \omega t$), such that $\Omega \gg \omega$. Further, we assume that the Bloch equations, as mentioned above in Eqs. (2.1)–(2.3), are lossless, i.e., the characteristic times for spin-spin and spin-lattice relaxation are too long compared to other timescales of the dynamics. Also, the length of the Bloch vector in Eqs. (2.1)–(2.3) is conserved, i.e.,

$$x^2 + y^2 + z^2 = 1. \quad (2.5)$$

From Eq. (2.5), it follows that the total quantum probability is conserved for the dynamics even though the energy is not.

Thus x , y , and z are less than or equal to unity. We further assume that the excitation is not too hard for our case [$(g/\Omega) < 1$]. The above consideration shows that, up to a leading order, z can be approximated as $z \simeq 1 - \frac{x^2 + y^2}{2}$. This helps us to decouple z from the Bloch equations (2.1)–(2.3). The constant of motion as expressed in Eq. (2.5) permits us to reduce the dimension of the phase space from three to two. Although replacing z in Eqs. (2.1)–(2.3) as above is an approximation, the error involved can be estimated by keeping track of the small difference [$1 - (x^2 + y^2 + z^2)$] for this conservative dynamics. To keep this difference small [50], we need to restrict the parameter space such that $|X_s| \leq 1$, where $|X_s|$ is given by the expression (2.12). We have carried out the numerical simulations of Bloch equations (as done in Sec. IV) by taking into consideration these constraints on the parameter space to keep the error less than 0.1%. The nonlinear contributions which are mainly responsible for symmetry breaking in the effective quantum dynamics can thus be taken into account. Finally, we mention that the lossless Bloch equations under consideration are free from the rotating wave approximation, commonly adopted for the majority of the treatments on atom-field dynamics.

We now introduce three parameters, which denote the strength of the atom-field interaction in terms of the amplitudes f_0 , c , and g in frequency units as follows:

$$\chi f_0 = \Omega_0, \quad \chi c = \omega_c, \quad \chi g = G. \quad (2.6)$$

Thus the dynamics can be controlled by four parameters, ω_0 , Ω_0 , ω_c , and G , where Ω_0 , ω_c , and G denote the Rabi frequencies which originate from the interaction between the two-level system and the three field components of $f(t)$. We also note that Eqs. (2.1)–(2.3) are linear and the forcing term $f(t)$ is multiplicative rather than additive, unlike the usual treatments of classical vibrational resonance.

B. Separation of the timescales and the slow dynamics

Let us proceed further with the Bloch equations (2.1)–(2.3). We differentiate Eq. (2.1) and use the normalization condition as mentioned in Eq. (2.5). A simple algebraic manipulation and elimination of z yields

$$\ddot{x} + \omega_0^2 x = F(t) \left[\frac{\omega_0}{2} x^2 + \frac{1}{2\omega_0} \dot{x}^2 - \omega_0 \right], \quad (2.7)$$

where $F(t) = [\Omega_0 + \omega_c \cos(\omega t) + G \cos(\Omega t)]$. As mentioned earlier, we must note that, even though the Bloch equations (2.1)–(2.3) are linear with three phase space variables, the reduction of the phase space dimension to two by using normalization condition Eq. (2.5) makes the dynamics nonlinear. Furthermore, we introduce two distinct timescales since $\Omega \gg \omega$ so that the dynamics becomes amenable to the theoretical scheme of vibrational resonance. Let us now proceed in the usual way [23,24,28,50] to split the variable x into a slow part $X(t, \omega t)$ and a fast part $\psi(t, \Omega t)$, such that $x(t) = X(t, \omega t) + \psi(t, \Omega t)$. Averaging over the fast component, we find

the slow dynamics as follows:

$$\begin{aligned}\ddot{X} + \omega_0^2 X &= -\omega_0 \Omega_0 - \omega_0 \omega_c \cos(\omega t) + \frac{\omega_0 G}{2} [X^2 \langle \cos(\Omega t) \rangle + 2X \langle \psi \cos(\Omega t) \rangle] \\ &+ \frac{\omega_0 \Omega_0}{2} [X^2 + 2X \langle \psi \rangle] + \frac{\omega_0 \omega_c \cos(\omega t)}{2} [X^2 + \langle \psi^2 \rangle + 2X \langle \psi \rangle] + \frac{\Omega_0}{2\omega_0} [\dot{X}^2 + 2\dot{X} \langle \dot{\psi} \rangle] \\ &+ \frac{\omega_c \cos(\omega t)}{2\omega_0} [\dot{X}^2 + 2\dot{X} \dot{\psi} + \langle \dot{\psi}^2 \rangle] + \frac{G}{2\omega_0} [\dot{X}^2 \langle \cos(\Omega t) \rangle + 2\dot{X} \langle \dot{\psi} \cos(\Omega t) \rangle].\end{aligned}\quad (2.8)$$

Similarly, the fast dynamics can be written as

$$\begin{aligned}\ddot{\psi} + \omega_0^2 \psi &= -\omega_0 G \cos(\Omega t) + \frac{\omega_0 \omega_c \cos(\omega t)}{2} [\psi^2 - \langle \psi^2 \rangle + 2X(\psi - \langle \psi \rangle)] \\ &+ \frac{\omega_0 \Omega_0}{2} [\psi^2 + 2X(\psi - \langle \psi \rangle)] + \frac{\Omega_0}{2\omega_0} [\dot{\psi}^2 + 2\dot{X}(\dot{\psi} - \langle \dot{\psi} \rangle)] \\ &+ \frac{\omega_0 G}{2} [\psi^2 \cos(\Omega t) + X^2 \{\cos(\Omega t) - \langle \cos(\Omega t) \rangle\} + 2X \{\psi \cos(\Omega t) - \langle \psi \cos(\Omega t) \rangle\}] \\ &+ \frac{G}{2\omega_0} [\dot{\psi}^2 \cos(\Omega t) + \dot{X}^2 \{\cos(\Omega t) - \langle \cos(\Omega t) \rangle\} + 2\dot{X} \{\dot{\psi} \cos(\Omega t) - \langle \dot{\psi} \cos(\Omega t) \rangle\}] \\ &+ \frac{\omega_c \cos(\omega t)}{2\omega_0} [\{\dot{\psi}^2 - \langle \dot{\psi}^2 \rangle\} + 2\dot{X} \{\dot{\psi} - \langle \dot{\psi} \rangle\}].\end{aligned}\quad (2.9)$$

We ignore the nonlinear contributions in Eq. (2.9) and assume $\ddot{\psi} \gg \psi, \dot{\psi}, \psi^2, \psi^3$. Thus its solution is given by

$$\psi = \frac{\omega_0 G}{\Omega^2} \cos(\Omega t).\quad (2.10)$$

Correspondingly, we obtain $\langle \psi \rangle = \langle \dot{\psi} \rangle = 0$, $\langle \psi^2 \rangle = \frac{\omega_0^2 G^2}{2\Omega^2}$, and $\langle \psi \cos(\Omega t) \rangle = \frac{\omega_0 G}{2\Omega}$. Substitution of the averages in Eq. (2.8) and on simplification, we obtain the slow dynamics as follows:

$$\begin{aligned}\ddot{X} + \left[\omega_0^2 - \frac{\omega_0^2 G^2}{2\Omega^2} \right] X &- \left[\frac{\omega_0 \Omega_0}{2} + \frac{\omega_0 \omega_c}{2} \cos(\omega t) \right] X^2 - \left[\frac{\Omega_0}{2\omega_0} + \frac{\omega_c}{2\omega_0} \cos(\omega t) \right] \dot{X}^2 \\ &= -\omega_0 \Omega_0 - \omega_0 \omega_c \cos(\omega t) + \frac{\omega_0 \omega_c}{4} \left\{ \frac{\omega_0^2 G^2}{\Omega^4} + \frac{G^2}{\Omega^2} \right\} \cos(\omega t).\end{aligned}\quad (2.11)$$

We now locate the steady state X_s of the dynamics by setting $\dot{X} = \ddot{X} = 0$, where

$$X_s = \frac{1}{2\Omega_0} \left\{ \left[2\omega_0 - \frac{\omega_0 G^2}{\Omega^2} \right] \pm \sqrt{\left[2\omega_0 - \frac{\omega_0 G^2}{\Omega^2} \right]^2 + 8\Omega_0^2} \right\}.\quad (2.12)$$

We must take care that $|X_s| \leq 1$ to validate the normalization condition. On perturbation Y ($Y = X - X_s$) about the steady state, the evolution of slow dynamics takes the following form:

$$\begin{aligned}\ddot{Y} + \left[\omega_0^2 - \frac{\omega_0^2 G^2}{2\Omega^2} - \omega_0 \Omega_0 X_s - \omega_0 \omega_c \cos \omega t \right] Y &- \left[\frac{\omega_0 \Omega_0}{2} + \frac{\omega_0 \omega_c}{2} \cos \omega t \right] Y^2 - \left[\frac{\Omega_0}{2\omega_0} + \frac{\omega_c}{2\omega_0} \cos \omega t \right] \dot{Y}^2 \\ &= \frac{\omega_c \omega_0}{4} \left[\frac{\omega_0^2 G^2}{\Omega^4} + \frac{G^2}{\Omega^2} - 4 + 2X_s^2 \right] \cos \omega t.\end{aligned}\quad (2.13)$$

This equation describes the slow Bloch dynamics of a (high frequency) field-dressed two-level system driven by a weak field and forms the basis of the rest of the treatment.

C. Perturbative analysis of the super- and subharmonic resonances: Stable and unstable zones

For convenience, we now rewrite the above equation as follows:

$$\ddot{q} + [\omega_1^2 - \epsilon \gamma \cos \omega_p t] q - \epsilon [\alpha_1 + \alpha_2 \cos \omega_p t] q^2 - \epsilon [\alpha_3 + \alpha_4 \cos \omega_p t] \dot{q}^2 = F \cos \omega_p t,\quad (2.14)$$

with the following abbreviations:

$$\begin{aligned}\omega_1^2 &= \left[\omega_0^2 - \frac{\omega_0^2 G^2}{2\Omega^2} - \omega_0 \Omega_0 X_s \right], \quad F = \frac{\omega_c \omega_0}{4} \left[\frac{\omega_0^2 G^2}{\Omega^4} + \frac{G^2}{\Omega^2} - 4 + 2X_s^2 \right], \\ \epsilon &= \frac{\omega_c}{G}, \quad \gamma = \omega_0 G, \quad \alpha_1 = \frac{\omega_0 \Omega_0 G}{2\omega_c}, \quad \alpha_2 = \frac{\omega_0 G}{2}, \quad \alpha_3 = \frac{\Omega_0 G}{2\omega_0 \omega_c}, \quad \alpha_4 = \frac{G}{2\omega_0}, \quad q = Y, \quad \omega_p = \omega.\end{aligned}$$

A comment on the smallness parameter ϵ , as introduced above, is pertinent. This factor is dimensionless and is used for bookkeeping in perturbative analysis particularly, to arrive at the solvability condition for removing secular divergence for each of the resonance cases. These conditions are independent of ϵ so that the amplitude-frequency profile (Arnold tongue) can be safely drawn for fixed values of G by keeping a check on the constraints on the parameter space as dictated by $|X_s| \leq 1$. This consideration is well vindicated by numerical simulations as discussed in Sec. IV.

Equation (2.14) is the central result of Sec. II on the basis of which we consider various resonances in the dynamics. This equation [47,48] can be identified as a forced nonlinear Mathieu equation, where parametric driving appears not only in the linear term but also in the nonlinear coefficients. The parametric excitations and the additive forcing are in the same phase. As the high frequency field has been averaged over, the dynamics is controlled by the weak field.

We first consider the linear dynamics. Equation (2.14) then reduces to

$$\ddot{q} + [\omega_1^2 - \epsilon \gamma \cos \omega_p t] q = F \cos \omega_p t, \quad (2.15)$$

which is a forced linear Mathieu equation. We shall return to it for further analysis in the next section. For the time being, we first note ϵ (the ratio of the strength of the low-frequency field to that for the high frequency field) $\ll 1$ and move on with all the nonlinear terms to proceed for deriving the perturbative equations order by order in ϵ in a general form.

By using the method of multiple scales [47] (MMS), we now search for the approximate solutions of Eq. (2.14). The

existence of various subharmonic and superharmonic resonances can be explored from this analysis. We wish to unravel these resonances systematically. The method of multiple scaling takes care of two timescales, a fast and a slow one, and correspondingly the variations in amplitude. Using MMS, we introduce fast and slow timescales T_0 and T_1 , respectively. Thus we have a dominant solution q_0 (zeroth order) and a perturbed solution q_1 (first order), in such a way that

$$q = q_0(T_0, T_1) + \epsilon q_1(T_0, T_1).$$

On substitution in Eq. (2.14), we have

$$\begin{aligned} [D_0^2 q_0 + \omega_1^2 q_0] + \epsilon [D_0^2 q_1 + \omega_1^2 q_1 + 2D_0 D_1 q_0 \\ - \gamma q_0 \cos \omega_p t] - \epsilon [\alpha_1 + \alpha_2 \cos \omega_p t] q_0^2 \\ - \epsilon [\alpha_3 + \alpha_4 \cos \omega_p t] \dot{q}_0^2 = F \cos \omega_p t, \end{aligned} \quad (2.16)$$

where the following notations have been used: $T_i = \epsilon^i T_0$, $\frac{d}{dt} = D_0 + \epsilon D_1$, and $D_i = \frac{d}{dT_i}$. We now compare the coefficients of the different powers of ϵ from both sides of Eq. (2.16). Thus, for the zeroth order (i.e., for ϵ^0), we obtain

$$D_0^2 q_0 + \omega_1^2 q_0 = F \cos \omega_p T_0. \quad (2.17)$$

Its solution can be written down as

$$q_0 = A e^{i\omega_1 T_0} + \lambda e^{-i\omega_p T_0} + \bar{A} e^{-i\omega_1 T_0} + \lambda e^{i\omega_p T_0}, \quad (2.18)$$

where $\lambda = \frac{F}{2(\omega_p^2 - \omega_1^2)}$ and the overbar denotes the complex conjugate. Similarly, for the first order of ϵ , we find

$$D_0^2 q_1 + \omega_1^2 q_1 = -2D_0 D_1 q_0 + \gamma q_0 \cos \omega_p t - \alpha_1 q_0^2 - \alpha_2 q_0^2 \cos \omega_p t - \alpha_3 \dot{q}_0^2 - \alpha_4 \dot{q}_0^2 \cos \omega_p t. \quad (2.19)$$

We substitute the solution for q_0 from Eq. (2.18) and expand the terms on the right hand side of Eq. (2.19). Our aim is to get rid of the coefficients of $e^{i\omega_1 T_0}$ which constitute the secular terms and make the solutions unbounded. Thus the solvability condition can be established by equating the coefficients of $e^{i\omega_1 T_0}$ terms to zero.

To proceed further, we expose the right hand side of Eq. (2.19) by substituting q_0 from Eq. (2.18) in it. This yields

$$\begin{aligned} D_0^2 q_1 + \omega_1^2 q_1 = & -2D_0 D_1 q_0 + \gamma q_0 \cos \omega_p t - \alpha_1 q_0^2 - \alpha_2 q_0^2 \cos \omega_p t - \alpha_3 \dot{q}_0^2 - \alpha_4 \dot{q}_0^2 \cos \omega_p t \\ = & -i\omega_1 [2A' e^{i\omega_1 T_0} - 2\bar{A}' e^{-i\omega_1 T_0}] + \frac{\gamma}{2} [A e^{i(\omega_p + \omega_1) T_0} + A e^{-i(\omega_p - \omega_1) T_0} \\ & + \lambda + \lambda e^{-2i\omega_p T_0} + \bar{A} e^{i(\omega_p - \omega_1) T_0} + \bar{A} e^{-i(\omega_p + \omega_1) T_0} + \lambda e^{2i\omega_p T_0} + \lambda] \\ & - \alpha_1 [A^2 e^{2i\omega_1 T_0} + \lambda^2 e^{-2i\omega_p T_0} + \bar{A}^2 e^{-2i\omega_1 T_0} + \lambda^2 e^{2i\omega_p T_0} + 2A\lambda e^{-i(\omega_p - \omega_1) T_0} \\ & + 2\bar{A}\lambda e^{-i(\omega_p + \omega_1) T_0} + 2A\bar{A} + 2A\lambda e^{i(\omega_p + \omega_1) T_0} + 2\lambda^2 + 2\bar{A}\lambda e^{i(\omega_p - \omega_1) T_0}] \\ & - \frac{\alpha_2}{2} [A^2 e^{i(\omega_p + 2\omega_1) T_0} + A^2 e^{-i(\omega_p - 2\omega_1) T_0} + \lambda^2 e^{-i\omega_p T_0} + \lambda^2 e^{-3i\omega_p T_0} \\ & + \bar{A}^2 e^{-i(\omega_p + 2\omega_1) T_0} + \lambda^2 e^{3i\omega_p T_0} + \lambda^2 e^{i\omega_p T_0} + 2A\lambda e^{i\omega_1 T_0} \\ & + 2A\lambda e^{-i(2\omega_p - \omega_1) T_0} + 2\bar{A}\lambda e^{-i\omega_p T_0} + 2A\lambda e^{i(2\omega_p + \omega_1) T_0} + 2A\lambda e^{i\omega_1 T_0} \\ & + 2\lambda^2 e^{i\omega_p T_0} + 2\lambda^2 e^{-i\omega_p T_0} + 2\bar{A}\lambda e^{i(2\omega_p - \omega_1) T_0} + 2\bar{A}\lambda e^{-i\omega_1 T_0}] \\ & + \alpha_3 [\omega_1^2 A^2 e^{2i\omega_1 T_0} + \omega_1^2 \bar{A}^2 e^{-2i\omega_1 T_0} - 2\omega_1^2 A\bar{A} + \lambda^2 \omega_p^2 e^{2i\omega_p T_0} + \lambda^2 \omega_p^2 e^{-2i\omega_p T_0} - 2\lambda^2 \omega_p^2 \end{aligned}$$

$$\begin{aligned}
& + 2\omega_1\omega_p\lambda\{A e^{i(\omega_p+\omega_1)T_0} - \bar{A} e^{i(\omega_p-\omega_1)T_0} - A e^{-i(\omega_p-\omega_1)T_0} + \bar{A} e^{-i(\omega_p+\omega_1)T_0}\}] \\
& + \frac{\alpha_4}{2}[\omega_1^2 A^2 e^{i(\omega_p+2\omega_1)T_0} + \omega_1^2 A^2 e^{-i(\omega_p-2\omega_1)T_0} + \omega_1^2 \bar{A}^2 e^{i(\omega_p-2\omega_1)T_0} + \omega_1^2 \bar{A}^2 e^{-i(\omega_p+2\omega_1)T_0} \\
& + 2\omega_1\omega_p\lambda\{A e^{i(2\omega_p+\omega_1)T_0} - \bar{A} e^{i(2\omega_p-\omega_1)T_0} - A e^{-i(2\omega_p-\omega_1)T_0} + \bar{A} e^{-i(2\omega_p+\omega_1)T_0}\} \\
& - 2\omega_1^2 A \bar{A} e^{i\omega_p T_0} - 2\omega_1^2 A \bar{A} e^{-i\omega_p T_0} + \lambda^2 \omega_p^2 e^{3i\omega_p T_0} - \lambda^2 \omega_p^2 e^{i\omega_p T_0} - \lambda^2 \omega_p^2 e^{-i\omega_p T_0} + \lambda^2 \omega_p^2 e^{-3i\omega_p T_0}]. \quad (2.20)
\end{aligned}$$

Here, the primes (') in A and \bar{A} refer to differentiation with respect to slow time T_1 . The above equation is the master equation for analyzing various resonances arising out of the driven dynamics. Since the high frequency field has already been averaged out and its effect is contained in the coefficients through its amplitude (G) and frequency (Ω), it is apparent that depending on the frequency of the weak driving field ω_p and the dressed frequency of the two-level system, ω_1 , the conditions for various superharmonic and subharmonic vibrational resonances can be worked out. In what follows in the next section, we analyze several such cases in detail.

III. VIBRATIONAL SUPER- AND SUBHARMONICS OF THE WEAK FIELD

A. Linear theory

In this section, we consider the dynamics governed by the linear terms of Eq. (2.14), i.e., Eq. (2.15), the linear forced Mathieu equation. We explore two types of resonances. The first one is the 1:2 superharmonic resonance, i.e., when the pumping frequency (ω_p) is around half that of the frequency of oscillation (ω_1) of the dressed two-level system. And the second one is the 2:1 subharmonic resonance, where the pumping frequency (ω_p) is twice that of the frequency of oscillation (ω_1). Our analysis is done separately for the two cases as follows.

1. Superharmonic resonance

As mentioned earlier, the pumping frequency (ω_p) is around half of the frequency of oscillation (ω_1); we consider $2\omega_p \simeq \omega_1$ or

$$2\omega_p = \omega_1 + \epsilon\sigma, \quad (3.1)$$

where σ is the detuning parameter and ϵ refers to the smallness parameter. The first two terms of Eq. (2.20) will contribute to the secular terms. Thus the coefficients of the term $e^{i\omega_1 T_0}$ for this particular case are $-i\omega_1(2A') + \frac{\gamma\lambda}{2}e^{i\sigma T_1}$. These secular terms must vanish for removal of the divergence. Hence the solvability condition can be obtained as follows:

$$i\omega_1(2A') - \frac{\gamma\lambda}{2}e^{i\sigma T_1} = 0. \quad (3.2)$$

Let us seek a trial solution of the form $A = \frac{1}{2}a e^{i\eta}$ and $\phi = \sigma T_1 - \eta$. Substituting in Eq. (3.2), we obtain

$$i\left[\omega_1 a' - \frac{\gamma\lambda}{2} \sin \phi\right] + \left[\omega_1 a(\phi' - \sigma) - \frac{\gamma\lambda}{2} \cos \phi\right] = 0. \quad (3.3)$$

Comparing the real and imaginary parts, we have

$$\begin{aligned}
\omega_1 a' &= \frac{\gamma\lambda}{2} \sin \phi, \\
\omega_1 a(\phi' - \sigma) &= \frac{\gamma\lambda}{2} \cos \phi. \quad (3.4)
\end{aligned}$$

For the steady state, we must set $a' = \phi' = 0$. Thus, from Eq. (3.4), we easily obtain σ as $\sigma = \pm \frac{\gamma\lambda}{4\omega_p a}$. From Eq. (3.1), we find

$$\omega_1 = 2\omega_p \mp \epsilon \left(\frac{\gamma\lambda}{4\omega_p a} \right). \quad (3.5)$$

The amplitude a can be determined approximately as follows. Identifying A as the amplitude of the undriven oscillator [Eq. (2.18)], its zeroth order contribution can be obtained from the energy $E = \frac{1}{2}\omega_1^2 a^2$ and, setting it equal to the energy of the two-level atom $\hbar\omega_0$ ($\hbar = 1$), we obtain $a = \sqrt{2/\omega_0}$ (assuming $\omega_0 \sim \omega_1$). Finally, in terms of our original system parameters, ω_0 , ω_p , ω_c , Ω , and G , Eq. (3.5) can be expressed as follows:

$$\begin{aligned}
& \left[\omega_0^2 - \frac{\omega_0^2 G^2}{2\Omega^2} - \omega_0 \Omega_0 X_s \right]^{1/2} \\
& = 2\omega_p \mp \omega_c \left\{ \frac{\omega_0^{3/2}}{8\sqrt{2}\omega_p (\omega_p^2 - \omega_1^2)} \frac{F}{\omega_1} \right\}. \quad (3.6)
\end{aligned}$$

A closer look at the above equation and the expression for X_s reveals that the occurrence of ω_0 on both sides of the algebraic equation makes the direct plot of the transition curves in the $\omega_0 - \omega_c$ plane difficult. We therefore fix the parameter values in Eq. (3.6) as $\omega_p = 1.0$, $\Omega = 10.0$ and for $G = 3.0$ to determine ω_0 and ω_c using the Newton-Raphson technique. We follow the same procedure for plotting the transition curves for other resonances as well. The V-shaped Arnold tongue depicting the stability zones under the 1:2 superharmonic resonance condition is shown in Fig. 1. Two transition curves emanate from the point ($\omega_1 [= \omega_0(1 - \frac{\omega_0^2 G^2}{2\Omega^2} - \omega_0 \Omega_0 X_s)^{1/2}]$, $\omega_c = 0$) on the ω_0 axis and define a region (II) of instability in between the two curves. Inside this region q grows exponentially for small values of ϵ (i.e., ω_c). Outside this tongue region q is the sum of terms, each of which is a product of two periodic functions. This implies that in these regions (I and III) we expect sustained sinusoidal oscillations under the superharmonic resonance ($\omega_1 \simeq 2\omega_p$) condition. We verify these theoretical predictions on the nature of the stability regions in the next section using detailed numerical simulations of the Bloch equations described by Eqs. (2.1)–(2.4) for several points marked in the stable and unstable regions in Fig. 1.

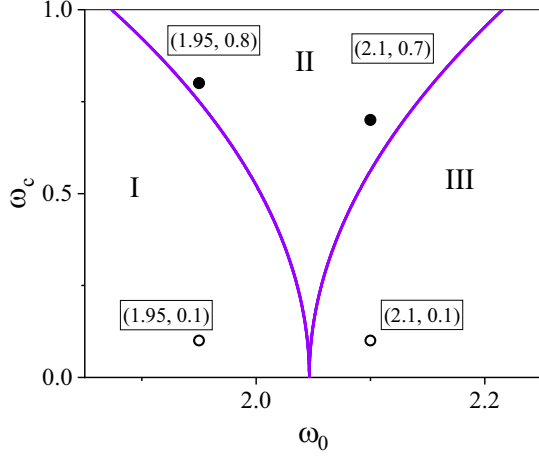


FIG. 1. V-shaped transition curves separating out the stability zones for $G = 3$ on the $\omega_c - \omega_0$ plane for $\omega_p = 1.0$, $\Omega = 10.0$ calculated theoretically [Eq. (3.6)] for a 1:2 superharmonic resonance condition. The region II lying inside a V-shaped curve is unstable, while the outside regions (I and III) are stable. The points marked in the stable and unstable regions are chosen for numerical simulation of the dynamics (units arbitrary).

2. Subharmonic resonance

In this case, the pumping frequency (ω_p) is twice the frequency of oscillation (ω_1); i.e., $\omega_p \simeq 2\omega_1$. Thus we consider

$$\omega_p = 2\omega_1 + \epsilon\sigma, \quad (3.7)$$

with σ and ϵ being the detuning parameter and the smallness parameter, respectively. Once again, the first two terms of Eq. (2.20) will contribute to the secular terms. Proceeding in the same way as in the previous case, and setting the coefficients of the secular terms equal to zero, we obtain the following solvability condition:

$$\left[i\omega_1(2A') - \frac{\gamma\bar{A}}{2} e^{i\sigma T_1} \right] = 0. \quad (3.8)$$

The trial solution of the form $A = \frac{1}{2}a e^{i\eta}$ with $\phi = \sigma T_1 - 2\eta$, in Eq. (3.8), yields

$$i \left[\omega_1 a' - \frac{\gamma A}{4} \sin \phi \right] + \left[\frac{\omega_1 a}{2} (\phi' - \sigma) - \frac{\gamma A}{4} \cos \phi \right] = 0. \quad (3.9)$$

Comparing the real and imaginary parts, we obtain as before

$$\omega_1 a' = \frac{\gamma A}{4} \sin \phi, \quad \omega_1 a (\phi' - \sigma) = \frac{\gamma A}{4} \cos \phi. \quad (3.10)$$

From here, we find σ as $\sigma = \pm \frac{\gamma}{\omega_p}$, by setting $a' = \phi' = 0$, for the steady state condition. Use of Eq. (3.7) leads us to $\omega_1 = (\omega_p/2) \mp \epsilon(\gamma/2\omega_p)$. We write down this expression, in terms of the original system parameters, as follows:

$$\left[\omega_0^2 - \frac{\omega_0^2 G^2}{2\Omega^2} - \omega_0 \Omega_0 X_s \right]^{1/2} = \frac{\omega_p}{2} \mp \omega_c \left(\frac{\omega_0}{2\omega_p} \right). \quad (3.11)$$

The transition curves are plotted in Fig. 2 on the $\omega_0 - \omega_c$ plane for the parameter values $\omega_p = 1.0$ and $\Omega = 10.0$ for

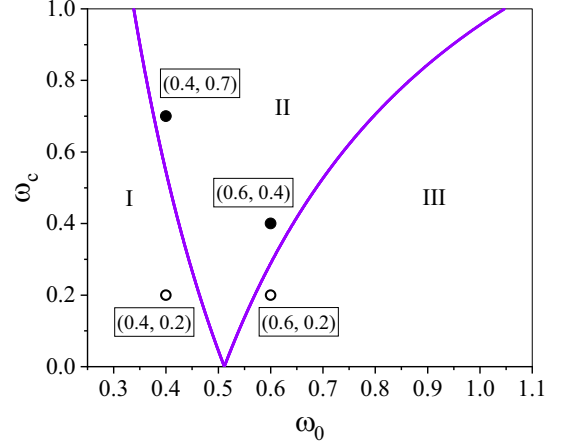


FIG. 2. Same as in Fig. 1, but calculated theoretically [Eq. (3.11)] for a 2:1 subharmonic resonance condition.

$G = 3.0$. The instability region II appears inside the tongue along with the stable oscillatory regions I and III under subharmonic resonance condition $\omega_1 = \omega_p/2$.

B. Inclusion of nonlinearity

We now move on to the next part, where all the nonlinear terms in Eq. (2.20) have been taken into consideration. Inclusion of nonlinearity enables us to explore some new cases of super- and subharmonic resonances, which could not be realized in the linear case. For instance, we explore here two more situations, namely, 1:3 superharmonic resonance, where the pumping frequency (ω_p) is close to one-third of the frequency of oscillation (ω_1), and the 3:1 subharmonic resonance, where the pumping frequency ω_p is about three times that of the frequency of oscillation ω_1 . In the following we discuss these two cases in detail.

1. Superharmonic resonance

The pumping frequency (ω_p) being around one-third of the frequency of oscillation ($\omega_1 \simeq 3\omega_p$) we consider

$$3\omega_p = \omega_1 + \epsilon\sigma. \quad (3.12)$$

From Eq. (2.20), we find the coefficients of the term $e^{i\omega_1 T_0}$. Since the coefficients of the secular terms must vanish, we have the following solvability condition:

$$[i\omega_1(2A') + 2\alpha_2 A \lambda + \alpha_6 e^{i\sigma T_1}] = 0, \quad (3.13)$$

where $\alpha_6 = \frac{\lambda^2}{2}(\alpha_2 - \alpha_4 \omega_p^2)$. Again assuming the trial solution $A = \frac{1}{2}a e^{i\eta}$ with $\phi = \sigma T_1 - \eta$ for Eq. (3.13), we find

$$i[\omega_1 a' + \alpha_6 \sin \phi] + [\omega_1 a (\phi' - \sigma) + \alpha_2 \lambda a + \alpha_6 \cos \phi] = 0. \quad (3.14)$$

We compare the real and imaginary parts of the last equation and set the condition for steady states $a' = \phi' = 0$ to obtain $\sigma = \frac{\alpha_2 \lambda}{3\omega_p} \pm \frac{\alpha_6}{3\omega_p a}$. Substitution of σ in Eq. (3.12) results in

$$\omega_1 = 3\omega_p - \omega_c \left[\frac{\lambda \omega_0}{6\omega_p} \pm \frac{\lambda^2}{12\omega_p \omega_0 a} (\omega_0^2 - \omega_p^2) \right]. \quad (3.15)$$

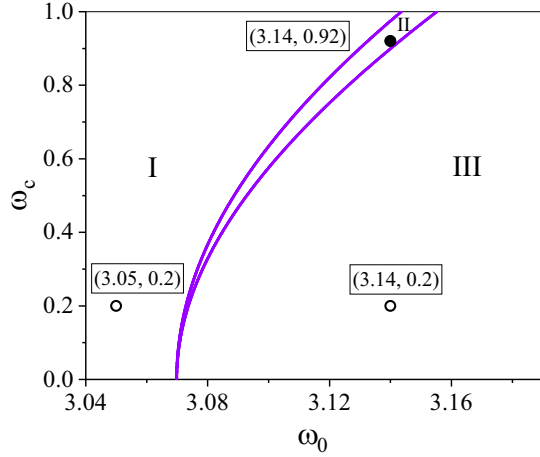


FIG. 3. V-shaped transition curve separating out the stability zones for $G = 3$ on the $\omega_c - \omega_0$ plane for $\omega_p = 1.0$, $\Omega = 10.0$, calculated theoretically [Eq. (3.16)] for 1:3 superharmonic resonance. The regions (I and III) outside a V-shaped curve are stable, while the region inside it (region II) is unstable. The points marked in the stable and unstable regions are chosen for numerical simulation of the dynamics (units arbitrary).

Finally, expressing Eq. (3.15) in terms of the original system parameters, we rewrite

$$\left[\omega_0^2 - \frac{\omega_0^2 G^2}{2\Omega^2} - \omega_0 \Omega_0 X_s \right]^{1/2} = 3\omega_p - \omega_c \left[\frac{\lambda \omega_0}{6\omega_p} \pm \frac{\lambda^2}{12\omega_p \omega_0 a} (\omega_0^2 - \omega_p^2) \right]. \quad (3.16)$$

The results on the transition curves for $\omega_p = 1.0$, $\Omega = 10.0$, and $G = 3.0$ are depicted in Fig. 3 for the superharmonic resonance condition $\omega_1 \simeq 3\omega_p$. It is interesting to note that, unlike the linear case, the transition curves here are tilted towards the right and the instability zone II inside the tongue region is narrowed down as a result of nonlinearity. The available regions for sustained superharmonic oscillations (regions I and III) appear to be wider. Finally, one may check that in the absence of nonlinearity this 1:3 superharmonic oscillation cannot be realized.

2. Subharmonic resonance

Finally we consider the case where the pumping frequency is around three times the frequency of oscillation, i.e., $\omega_1 \simeq \omega_p/3$. Thus we write

$$\omega_p = 3\omega_1 + \epsilon\sigma. \quad (3.17)$$

Once again, from Eq. (2.20), we find the coefficients of the secular term $e^{i\omega_1 T_0}$ and set them to zero for finite solutions. We find the solvability condition as

$$[i\omega_1(2A') + 2\alpha_2 A \lambda + 4\alpha_8 \bar{A}^2 e^{i\sigma T_1}] = 0, \quad (3.18)$$

where $\alpha_8 = \frac{1}{8}(\alpha_2 - \alpha_4 \omega_1^2)$. Assuming again the following form $A = \frac{1}{2} a e^{i\eta}$ with $\phi = \sigma T_1 - 3\eta$ and substituting in

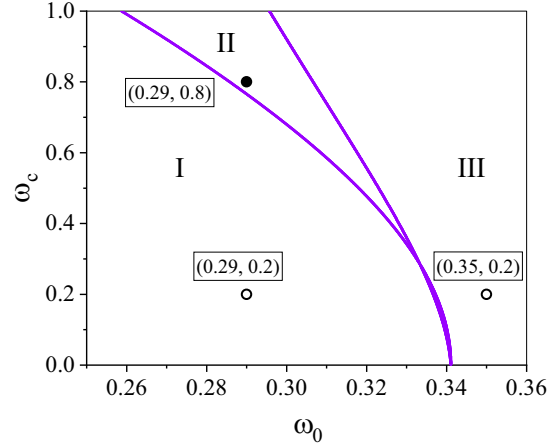


FIG. 4. Same as in Fig. 1, but calculated theoretically [Eq. (3.21)] for 3:1 subharmonic resonance.

Eq. (3.18), we arrive at the following equation:

$$i[\omega_1 a' + \alpha_8 a^2 \sin \phi] + \left[\frac{\omega_1 a}{3} (\phi' - \sigma) + \alpha_2 \lambda a + \alpha_8 a^2 \cos \phi \right] = 0. \quad (3.19)$$

Comparing the real and imaginary parts in the steady state, we find $\sigma = \frac{2}{\omega_p}(\alpha_2 \lambda \pm \alpha_8 a)$. Inclusion of σ in Eq. (3.17) results in

$$\omega_1 = \frac{\omega_p}{3} - \frac{3\omega_c}{\omega_p} \left[\frac{\omega_0 \lambda}{2} \pm \frac{a}{144\omega_0} (9\omega_0^2 - \omega_p^2) \right]. \quad (3.20)$$

Finally, we express the above relation in terms of the original system parameters:

$$\left[\omega_0^2 - \frac{\omega_0^2 G^2}{2\Omega^2} - \omega_0 \Omega_0 X_s \right]^{1/2} = \frac{\omega_p}{3} - \frac{3\omega_c}{\omega_p} \left[\frac{\omega_0 \lambda}{2} \pm \frac{a}{144\omega_0} (9\omega_0^2 - \omega_p^2) \right]. \quad (3.21)$$

Equation (3.21) is now used to draw the transition curves in the $\omega_0 - \omega_c$ plane for the 3:1 subharmonic case in Fig. 4 for the set of parameters $\omega_p = 1.0$, $\Omega = 10.0$, and $G = 3.0$. Here, the transition curves tilt towards the left. The instability region inside the tongue appears to be narrow. The nature of the stability patterns for the regions I and III in Fig. 4 clearly follows those for Fig. 3 as the effect of nonlinearity is very much pronounced.

IV. NUMERICAL SIMULATIONS OF SUPER- AND SUBHARMONIC VIBRATIONAL RESONANCES

A. Resonance oscillations and instability zones

Our theoretical analysis of the Bloch equations for a two-level system in bichromatic fields is based on the method of multiple timescales and averaging over the fast motion. We have shown that it is possible to identify the different stability regimes in the $\omega_0 - \omega_c$ plane for several superharmonic and subharmonic resonance cases. While in the stable region one is expected to observe sustained sinusoidal oscillations at the sub- or superharmonic frequency of the applied low frequency

field, the unstable regions are characterized by exponential divergence. This result is a consequence of the linear stability analysis. In actual practice, however, nonlinearity affects the dynamics in the following way. As the amplitude of motion increases due to resonance, the dependence of frequency on the amplitude causes the resonance to detune as a result of which the tendency of large amplitude motion is decreased. The exponential divergence in the unstable regime also gets smoothed out due to nonlinearity. As a result we expect complex multimode oscillatory dynamics but still bounded in this regime.

In this section we have carried out detailed numerical simulations of Eqs. (2.1)–(2.4) using the Runge-Kutta method for the set of parameters satisfying the condition $|X_s| \leq 1$, where X_s is given by Eq. (2.12) to corroborate our theoretical findings. To this end, we choose the parameter set $\omega_p = 1.0$ and $\Omega = 10.0$ and $G = 3.0$ as used for illustrating the theoretical transition curves in Figs. 1–4. Furthermore, we choose the step size $h = 0.001$ for numerical integration. Each of the resonance cases are explored as follows.

1. Superharmonic resonance

We return to Fig. 1 and select out several representative points in the distinct stability regions bounded by the V-shaped transition curves in the $\omega_0 - \omega_c$ plane. We begin by choosing a point ($\omega_0 = 1.95$, $\omega_c = 0.1$) from the stable region I, i.e., from the left side of the tongue, and observe sustained periodic oscillations of $x(t)$ with a time period which is half that of the weak driving field $\cos \omega_p t$. The waveform as a function of time is shown in Fig. 5(b). We have also chosen another point ($\omega_0 = 2.1$, $\omega_c = 0.1$) from the right side of the tongue in the stable region III to show the sustained periodic oscillation with the same time period [Fig. 5(c)]. For a comparison of the time period of oscillations we have also plotted the oscillation of the weak driving field with frequency ω_p in Fig. 5(a). Moving on to the unstable region (II) inside the tongue, we choose two different points at ($\omega_0 = 1.95$, $\omega_c = 0.8$) and ($\omega_0 = 2.1$, $\omega_c = 0.7$). It is evident that the dynamics is characterized by irregular complex multimode oscillations. The results are shown in Figs. 5(d) and 5(e), respectively. The parametric resonance oscillation can therefore be judiciously controlled by identifying the appropriate stability zones with the help of secular perturbative analysis of the high frequency field-dressed dynamical system.

2. Subharmonic resonance

To explore the dynamics under this resonance condition, we select the representative points in the $\omega_0 - \omega_c$ plane of Fig. 2 for the stable regimes I on the left of the transition curves ($\omega_0 = 0.4$, $\omega_c = 0.2$) and III on the right of the transition curves ($\omega_0 = 0.6$, $\omega_c = 0.2$) for numerical simulations. The results are shown in Figs. 6(b) and 6(c). The periodic oscillations at a frequency half that for the applied low frequency field ω_p are observed. For the selected points ($\omega_0 = 0.4$, $\omega_c = 0.7$) and ($\omega_0 = 0.6$, $\omega_c = 0.4$) in the unstable regime inside the tongue, we observe irregular multimode oscillations as shown in Figs. 6(d) and 6(e), as predicted from our theoretical analysis.

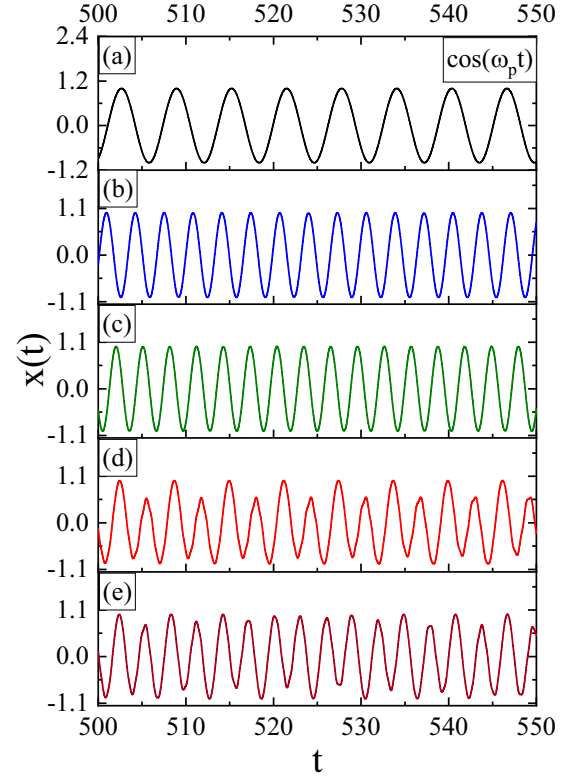


FIG. 5. Numerically simulated [Eqs. (2.1)–(2.4)] time series for a 1:2 superharmonic vibrational resonance for $G = 3$ for the points lying on the stable (I and III) and unstable regions (II) in the $\omega_0 - \omega_c$ plane of Fig. 1, for $\omega_p = 1.0$, $\Omega = 10.0$. (a) Oscillation of the applied weak periodic drive $\cos \omega_p t$ drawn for comparison of the time periods. (b) Resonance oscillation with time period 1/2 of the period of the weak driving field for the point ($\omega_0 = 1.95$, $\omega_c = 0.1$) in the stable region I of Fig. 1. (c) Resonance oscillation with time period 1/2 of the period of the weak driving field for the point ($\omega_0 = 2.1$, $\omega_c = 0.1$) in the stable region III of Fig. 1. (d) Irregular multimode oscillations corresponding to the point ($\omega_0 = 1.95$, $\omega_c = 0.8$) in the unstable region II of Fig. 1. (e) Irregular multimode oscillations corresponding to the point ($\omega_0 = 2.1$, $\omega_c = 0.7$) in the unstable region II of Fig. 1 (units arbitrary).

3. Superharmonic resonance

We now discuss this case with reference to $\omega_0 - \omega_c$ transition curves and stability zones as depicted in Fig. 3 on the basis of our theoretical analysis which takes care of the leading order nonlinearity. It follows that the instability zones inside the tongues are narrowed down as compared to earlier cases and the tongue gets tilted. Increased availability of the stable zones allows us to choose the representative points over a wide range for parametric superharmonic resonance oscillations. We select the points ($\omega_0 = 3.05$, $\omega_c = 0.2$) and ($\omega_0 = 3.14$, $\omega_c = 0.2$) in the stable regimes in Fig. 3 of the transition curves for numerical simulations. The time series for 1:3 superharmonic resonance oscillations are displayed in Figs. 7(b) and 7(c), respectively. The chosen point ($\omega_0 = 3.14$, $\omega_c = 0.92$) belongs to the unstable region inside the tongue for which Fig. 7(d) depicts the complex multimode

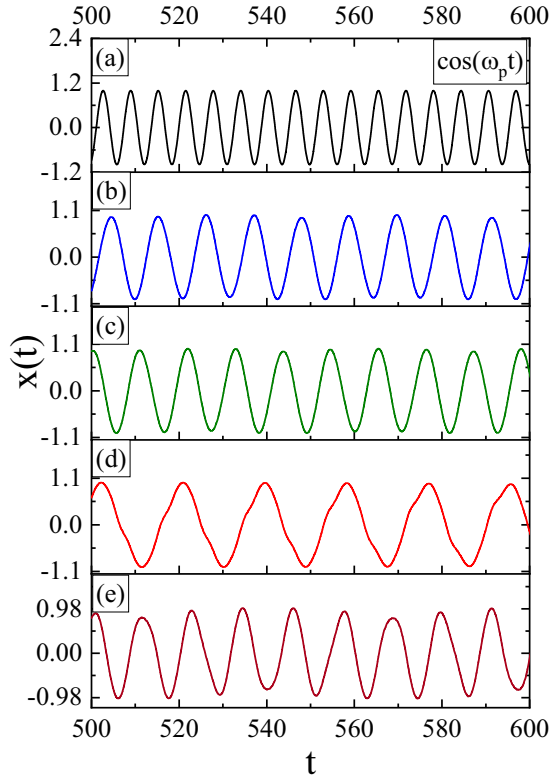


FIG. 6. Numerically simulated [Eqs. (2.1)–(2.4)] time series for a 2:1 subharmonic vibrational resonance for $G = 3$ for the points lying on the stable (I and III) and unstable (II) regions in the $\omega_0 - \omega_c$ plane of Fig. 2, for $\omega_p = 1.0$, $\Omega = 10.0$. (a) Oscillation of the applied weak periodic drive $\cos \omega_p t$ drawn for comparison of the time periods. (b) Resonance oscillation with a time period double that of the weak driving field for the point ($\omega_0 = 0.4$, $\omega_c = 0.2$) in the stable region I of Fig. 2. (c) Resonance oscillation with a time period almost double that of the weak driving field for the point ($\omega_0 = 0.6$, $\omega_c = 0.2$) in the stable region III of Fig. 2. (d) Irregular multimode oscillations corresponding to the point ($\omega_0 = 0.4$, $\omega_c = 0.7$) in the unstable region II of Fig. 2. (e) Irregular multimode oscillations corresponding to the point ($\omega_0 = 0.6$, $\omega_c = 0.4$) in the unstable region II of Fig. 2 (units arbitrary).

oscillation. As before, Fig. 7(a) refers to the weak pump field shown for comparison of the time periods.

4. Subharmonic resonance

We now move on to Fig. 4 displaying the transition curves to explore the 3:1 subharmonic parametric resonance oscillation condition. Here again the instability regions are narrowed down to a great extent and the transition curves tilt towards the left. Regular resonance oscillations are observed for numerical simulation of the dynamics for the points ($\omega_0 = 0.29$, $\omega_c = 0.2$) and ($\omega_0 = 0.35$, $\omega_c = 0.2$) selected from the stable regimes I and III of Fig. 4. The results are shown in Figs. 8(b) and 8(c), respectively. The point ($\omega_0 = 0.29$, $\omega_c = 0.8$) corresponds to the unstable region inside the tongue. The complex oscillation for this point is shown in Fig. 8(d). Figure 8(a) represents the sinusoidal oscillations for weak pump field ω_p , shown for the comparison of time periods.

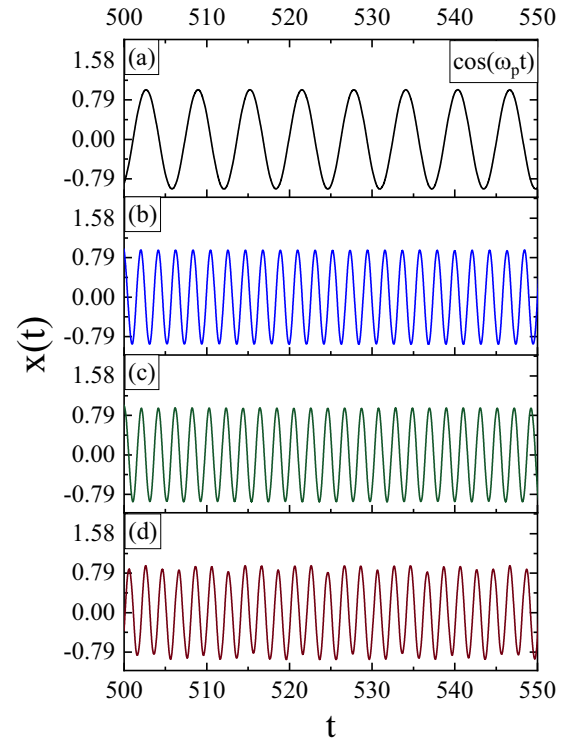


FIG. 7. Numerically simulated [Eqs. (2.1)–(2.4)] time series for a 1:3 superharmonic vibrational resonance for $G = 3$ for the points lying on the stable (I and III) and unstable (II) regions in the $\omega_0 - \omega_c$ plane of Fig. 3, for $\omega_p = 1.0$, $\Omega = 10.0$. (a) Oscillation of the applied weak periodic drive $\cos \omega_p t$ drawn for comparison of the time periods. (b) Resonance oscillation with a time period one-third (1/3) of the driving field for the point ($\omega_0 = 3.05$, $\omega_c = 0.2$) in the stable region I of Fig. 3. (c) Resonance oscillation with a time period one-third (1/3) of that of the driving field for the point ($\omega_0 = 3.14$, $\omega_c = 0.2$) in the stable region III of Fig. 3. (d) Irregular multimode oscillations corresponding to the point ($\omega_0 = 3.14$, $\omega_c = 0.92$) in the unstable region II of Fig. 3 (units arbitrary).

B. Effect of high frequency on the transition of stability

We now discuss the effect of high frequency (Ω) of the fast time-varying field on the stability zones as depicted in Figs. 1–4. A prototypical case, 1:2 superharmonic resonance, is considered. In Fig. 9, the V-shaped transition curves are plotted for $\Omega = 10$ (solid line) and $\Omega = 5$ (dotted line) for $\omega_p = 1.0$, $G = 3.0$. As Ω is lowered the tongue moves to the right. It therefore follows that a part of the region which remains as a stable zone for $\Omega = 10$ becomes unstable for $\Omega = 5$ since the concerned region falls inside the tongue for the later case. To be more specific, we consider a point ($\omega_0 = 2.2$, $\omega_c = 0.2$) on the $\omega_0 - \omega_c$ plane which is stable for $\Omega = 10$ but unstable for $\Omega = 5$ and numerically simulate the Bloch dynamics. The results are shown in Fig. 10. We observe sustained periodic 1:2 superharmonic oscillation [Fig. 10(b)] for $\Omega = 10$. For $\Omega = 5$, the dynamics turns out to be multimode complex oscillatory [Fig. 10(c)] in nature, vindicating our theoretical predictions. We observe a similar effect of high frequency (Ω) on the transition of stability in other super- and subharmonic cases. However, for the sake of brevity we have not reproduced them in this paper.

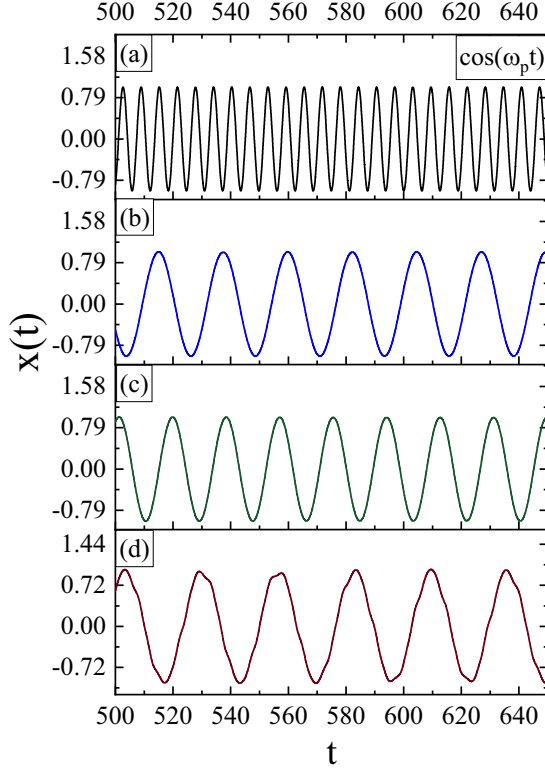


FIG. 8. Numerically simulated [Eqs. (2.1)–(2.4)] time series for a 3:1 subharmonic vibrational resonance for $G = 3$ for the points lying on the stable and unstable regions in the $\omega_0 - \omega_c$ plane of Fig. 4, for $\omega_p = 1.0$, $\Omega = 10.0$. (a) Oscillation of the applied weak periodic drive $\cos \omega_p t$ drawn for comparison of the time periods. (b) Resonance oscillation with a time period three times that of the weak driving field for the point ($\omega_0 = 0.29$, $\omega_c = 0.2$) in the stable region I of Fig. 4. (c) Resonance oscillation with a time period three times that of the weak driving field for the point ($\omega_0 = 0.35$, $\omega_c = 0.2$) in the stable region III of Fig. 4. (d) Irregular multimode oscillations corresponding to the point ($\omega_0 = 0.29$, $\omega_c = 0.8$) in the unstable region II of Fig. 4 (units arbitrary).

C. Vibrational super- and subharmonic response

Finally, we calculate numerically the response of the two-level system dressed by the high frequency field to the weak driving field ($\omega_c \cos \omega_p t$) at the subharmonics and superharmonics of the weak field. The sine and cosine components $B_s(f)$ and $B_c(f)$, respectively, of the polarization variable $x(t)$ of the Bloch equations [Eqs. (2.1)–(2.4)] are defined [20] as

$$B_s(f) = \frac{2}{nT} \int_0^{nT} x(t) \sin(ft) dt, \quad (4.1)$$

$$B_c(f) = \frac{2}{nT} \int_0^{nT} x(t) \cos(ft) dt, \quad (4.2)$$

where $T = 2\pi/f$ with integer n . Based on the numerical integration of Eqs. (2.1)–(2.4), which yield $x(t)$, one determines the linear response function for $f = 2\omega_p$ (1:2 superharmonic resonance), $f = \omega_p/2$ (2:1 subharmonic resonance), $f = 3\omega_p$ (1:3 superharmonic resonance), and $f = \omega_p/3$ (3:1 subhar-

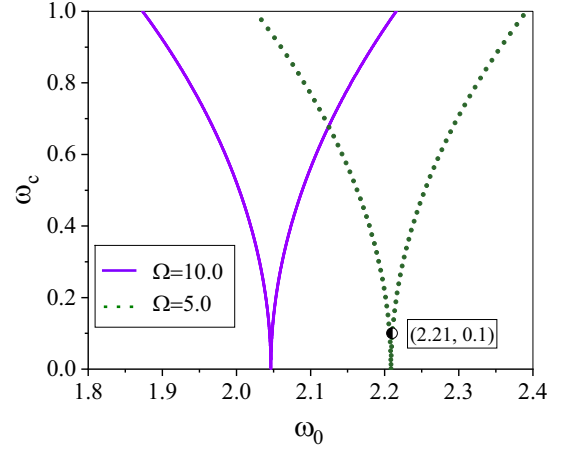


FIG. 9. V-shaped transition curves separating out the stability zones for $\Omega = 10$ (solid line) and $\Omega = 5$ (dotted line) on the $\omega_c - \omega_0$ plane for $\omega_p = 1.0$, $G = 3$, calculated theoretically [Eq. (3.6)] for a 1:2 superharmonic resonance. The point marked at $\omega_0 = 2.21$, $\omega_c = 0.1$ lies on the stable region for $\Omega = 10$, but on the unstable dynamics for $\Omega = 5$ and is chosen for numerical simulations of the dynamics presented in Fig. 10 (units arbitrary).

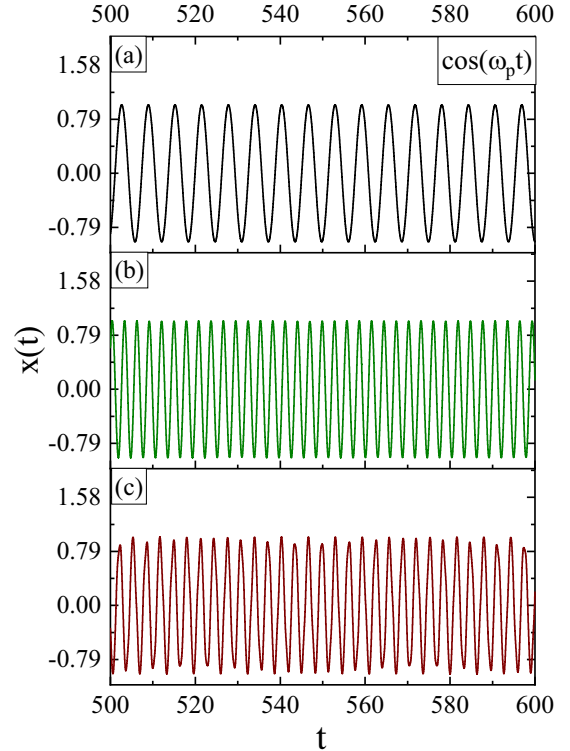


FIG. 10. Effect of high frequency Ω on the stability zones: numerically simulated [Eqs. (2.1)–(2.4)] time series for a 1:2 superharmonic resonance for the point ($\omega_0 = 2.21$, $\omega_c = 0.1$) lying in the $\omega_0 - \omega_c$ plane of Fig. 9 for $\omega_p = 1.0$, $G = 3$. (a) Oscillation of the periodic drive $\cos \omega_p t$ drawn for comparison of the time periods. (b) Resonance oscillation with a time period half that of the period of the weak driving field for $\Omega = 10$. (c) Complex multimode oscillation for $\Omega = 5$ (units arbitrary).

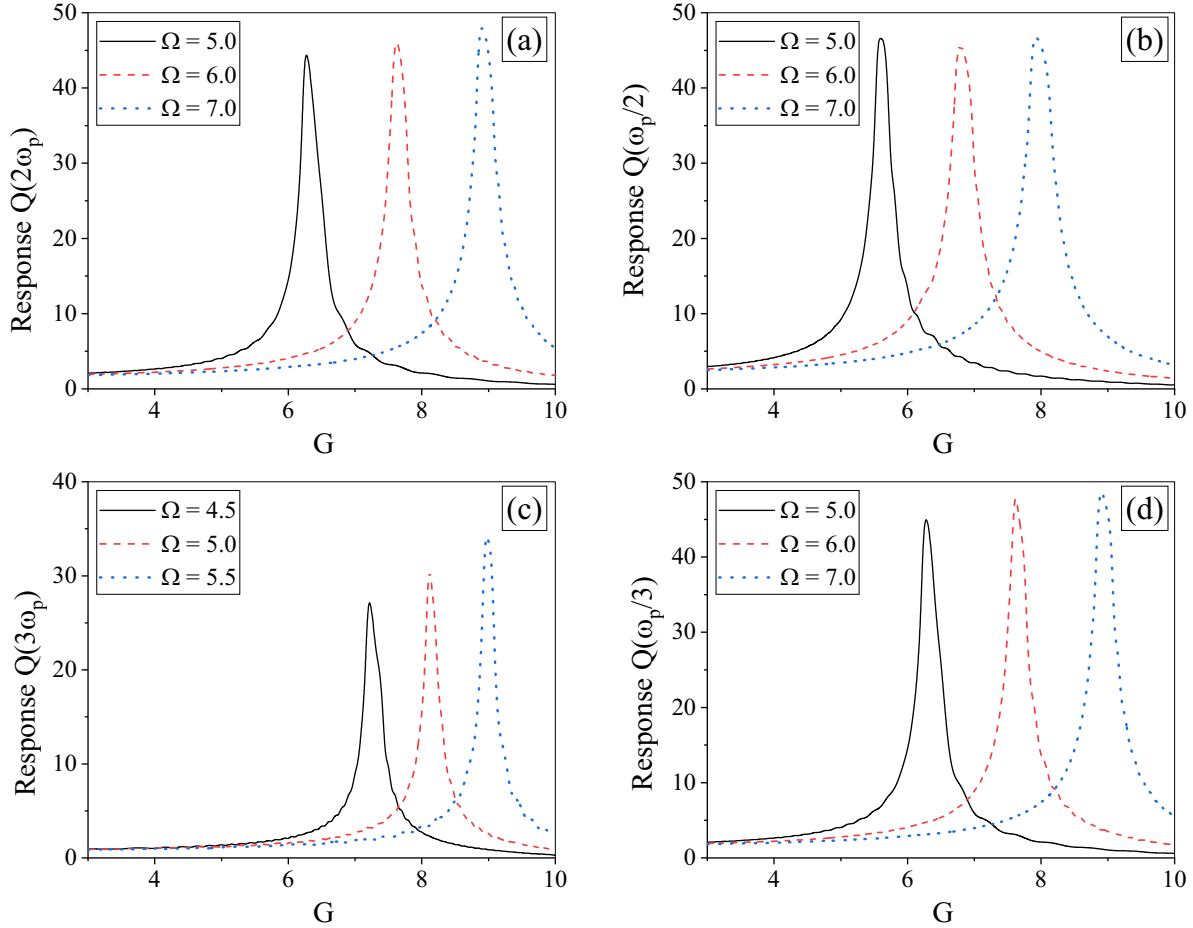


FIG. 11. Vibrational resonance enhancement of weak super- and subharmonic signals. (a) The numerical plot of the response $Q(2\omega_p)$ versus high frequency amplitude ($\omega_p = 0.5$, $\omega_0 = 1.0$) for a 1:2 superharmonic resonance for several values of Ω . (b) Same as in (a) but for $Q(\omega_p/2)$ for a 2:1 subharmonic resonance ($\omega_p = 1.8$, $\omega_0 = 0.9$). (c) Same as in (a) but for $Q(3\omega_p)$ for a 1:3 superharmonic resonance ($\omega_p = 0.5$, $\omega_0 = 1.5$). (d) Same as in (a) but for $Q(\omega_p/3)$ for a 3:1 subharmonic resonance ($\omega_p = 3.0$, $\omega_0 = 1.0$) (units arbitrary).

monic resonance) as the following:

$$Q(f) = \frac{\sqrt{B_s(f)^2 + B_c(f)^2}}{\omega_c/\chi}. \tag{4.3}$$

The resonance response functions $Q(2\omega_p)$, $Q(\omega_p/2)$, $Q(3\omega_p)$, $Q(\omega_p/3)$ vs G , the strength of the high-frequency field, are plotted in Figs. 11(a)–11(d) for several values of Ω . In each case, we observe a bell-shaped curve that depicts the enhancement of the response signal corresponding to the resonance. The variation of the maximum value of G against Ω is found to be linear as found in many other cases of vibrational resonance [20–24].

V. CONCLUSION

In this paper, we have examined the Bloch dynamics of a two-level quantum system in bichromatic fields comprised of a fast time-periodic field and a slow one. The main idea is the search for nonlinear resonances in a fast-field-dressed system associated with instability. To put the present work in the appropriate perspective we note the two pertinent points. First, the dynamics of a quantum system driven by

two time-periodic fields lies at the heart of several branches of spectroscopy [41,51], e.g., double resonance, pump probe, wave mixing, etc. A conspicuous feature in the treatment of these photophysical processes is the use of a high intensity field (rather than a high frequency field) as the pump and the weak field as a probe. When the material medium is considered to be active the energy levels get dressed by the intense field. Furthermore, in the nonlinear optics [51] with passive media one considers the generation of harmonics, sum, and difference frequency field, where one of the two fields is intense. The quantum dynamics in the present context, on the other hand, concerns the field-dressed levels where the field is characteristically of high frequency but the excitation is not too hard. Thus the separation of timescales plays a major role and the effect of the high-frequency field which mimics a noise is subsumed in the dynamics by averaging over the fast timescale. Secondly, the use of a normalization condition enables us to reduce the dimension of the phase space of the dynamics from three to two and in the process brings forth nonlinearity in the scheme. An interplay of this nonlinearity and the high frequency field results in the reduced dynamics in the form of a forced nonlinear Mathieu

equation. We have demonstrated how the linear and non-linear response of the system to the weak probe field can be realized as regular sustained oscillations at the subharmonic or superharmonic frequency of the weak field in the stable zone in the frequency-amplitude plot well separated from the unstable region of the Arnold tongue. It has been shown how the responses can be enhanced by optimizing the strength and frequency of the fast time-varying field. The detailed numerical simulation of the Bloch equations vindicates our theoretical analysis. We believe that the generation of subharmonic and superharmonic frequency of a weak probe as proposed here can be achieved experimentally in a standard quantum optical setup with quantum dots [52].

Quantum optics, in general, can be a convenient platform for experimental studies of vibrational enhancement of weak signals.

ACKNOWLEDGMENTS

Thanks are due to the Science and Engineering Research Board, the Department of Science and Technology, Government of India for support through a J. C. Bose National Fellowship (D.S.R.) and a research associateship (P.S.) under Grant No. SB/ S2/JCB-030/2015 and to the University Grants Commission, Government of India (S.P.) for partial financial support.

-
- [1] R. Benzi, G. Parisi, A. Sutera, and A. Vulpiani, *Tellus* **34**, 10 (1982).
 - [2] R. Benzi, A. Sutera, and A. Vulpiani, *J. Phys. A: Math. Gen.* **14**, L453 (1981).
 - [3] S. Fauve and F. Heslot, *Phys. Lett. A* **97**, 5 (1983).
 - [4] B. McNamara, K. Wiesenfeld, and R. Roy, *Phys. Rev. Lett.* **60**, 2626 (1988).
 - [5] L. Gammaitoni, P. Hänggi, P. Jung, and F. Marchesoni, *Rev. Mod. Phys.* **70**, 223 (1998).
 - [6] C. R. Doering and J. C. Gadoua, *Phys. Rev. Lett.* **69**, 2318 (1992).
 - [7] M. Marchi, F. Marchesoni, L. Gammaitoni, E. Menichella-Saetta, and S. Santucci, *Phys. Rev. E* **54**, 3479 (1996).
 - [8] P. K. Ghosh and D. S. Ray, *J. Chem. Phys.* **125**, 124102 (2006).
 - [9] A. S. Pikovsky and J. Kurths, *Phys. Rev. Lett.* **78**, 775 (1997).
 - [10] D. E. Postnov, S. K. Han, T. G. Yim, and O. V. Sosnovtseva, *Phys. Rev. E* **59**, R3791(R) (1999).
 - [11] C. Zeng, C. Zhang, J. Zeng, R. Liu, and H. Wang, *J. Stat. Mech.* (2015) P08027.
 - [12] C. Van den Broeck, J. M. R. Parrondo, and R. Toral, *Phys. Rev. Lett.* **73**, 3395 (1994).
 - [13] A. Sanz-Anchergues, A. M. Zhabotinsky, I. R. Epstein, and A. P. Muñuzuri, *Phys. Rev. E* **63**, 056124 (2001).
 - [14] S. Dutta, S. S. Riaz, and D. S. Ray, *Phys. Rev. E* **71**, 036216 (2005).
 - [15] F. Sagués, J. M. Sancho, and J. García-Ojalvo, *Rev. Mod. Phys.* **79**, 829 (2007).
 - [16] D. Das and D. S. Ray, *Phys. Rev. E* **87**, 062924 (2013).
 - [17] A. Guderian, G. Dechert, K. P. Zeyer, and F. W. Schneider, *J. Phys. Chem.* **100**, 4437 (1996).
 - [18] L. M. Ward, S. M. Doesburg, K. Kitajo, S. E. MacLean, and A. B. Roggeveen, *Can. J. Exp. Psychol.* **60**, 319 (2006).
 - [19] F. Moss, L. M. Ward, and W. G. Sannita, *Clin. Neurophysiol.* **115**, 267 (2004).
 - [20] P. S. Landa and P. V. E. McClintock, *J. Phys. A: Math. Gen.* **33**, L433 (2000).
 - [21] M. Gitterman, *J. Phys. A: Math. Gen.* **34**, L355 (2001).
 - [22] A. A. Zaikin, L. López, J. P. Baltanás, J. Kurths, and M. A. F. Sanjuán, *Phys. Rev. E* **66**, 011106 (2002).
 - [23] I. I. Blekhman and P. S. Landa, *Int. J. Non-Linear Mech.* **39**, 421 (2004).
 - [24] A. Ichiki, Y. Tadokoro, and M. Takanashi, *J. Phys. A: Math. Theor.* **45**, 385101 (2012).
 - [25] V. N. Chizhevsky, E. Smeu, and G. Giacomelli, *Phys. Rev. Lett.* **91**, 220602 (2003).
 - [26] V. N. Chizhevsky and G. Giacomelli, *Phys. Rev. E* **73**, 022103 (2006).
 - [27] V. N. Chizhevsky, *Phys. Rev. E* **90**, 042924 (2014).
 - [28] J. P. Baltanás, L. López, I. I. Blechman, P. S. Landa, A. Zaikin, J. Kurths, and M. A. F. Sanjuán, *Phys. Rev. E* **67**, 066119 (2003).
 - [29] L. Du, R. Han, J. Jiang, and W. Guo, *Phys. Rev. E* **102**, 012149 (2020).
 - [30] R. Gui, Y. Wang, Y. Yao, and G. Cheng, *Chaos Solitons Fractals* **138**, 109952 (2020).
 - [31] P. Sarkar and D. S. Ray, *Phys. Rev. E* **99**, 052221 (2019).
 - [32] S. Rajamani, S. Rajasekar, and M. A. F. Sanjuán, *Commun. Nonlin. Sci. Numer. Simul.* **19**, 4003 (2014).
 - [33] S. Ghosh and D. S. Ray, *Phys. Rev. E* **88**, 042904 (2013).
 - [34] D. Das and D. S. Ray, *Eur. Phys. J. B* **91**, 279 (2018).
 - [35] M. Borromeo and F. Marchesoni, *Phys. Rev. E* **73**, 016142 (2006).
 - [36] U. E. Vincent, P. V. E. McClintock, I. A. Khovanov, S. Rajasekar, *Philos. Trans. R. Soc. A* **379**, 20200226 (2021); **379**, 20210003 (2021).
 - [37] S. Rajasekar and M. A. F. Sanjuán, *Nonlinear Resonances (Springer Series in Synergetics)* (Springer, Switzerland, 2016).
 - [38] O. I. Olusola, O. P. Shomotun, U. E. Vincent, and P. V. E. McClintock, *Phys. Rev. E* **101**, 052216 (2020).
 - [39] S. Ghosh and D. S. Ray, *Eur. Phys. J. B* **88**, 23 (2015).
 - [40] C. P. Slichter, *Principles of Magnetic Resonance*, 3rd ed. (Springer, New York, 1996).
 - [41] M. Sargent, M. O. Scully, and W. E. Lamb, *Laser Physics* (Addison-Wesley, New York, 1987).
 - [42] L. Allen and J. H. Eberly, *Optical Resonance and Two-Level Atoms* (Dover Publications, Mineola, NY, 1987).
 - [43] H. C. Torrey, *Phys. Rev.* **104**, 563 (1956).
 - [44] S. L. McCall and E. L. Hahn, *Phys. Rev.* **183**, 457 (1969).
 - [45] J. R. Ackerhalt, P. W. Milonni, and M.-L. Shih, *Phys. Rep.* **128**, 205 (1985).
 - [46] A. Nath and D. S. Ray, *Phys. Rev. A* **36**, 431(R) (1987).
 - [47] R. H. Rand, *Lecture Notes on Nonlinear Vibrations* (Version 53) (Cornell University, Ithaca, NY, 2017), p. 14853.

- [48] I. Kovacic, R. Rand, and S. M. Sah, [Appl. Mech. Rev. **70**, 020802 \(2018\)](#).
- [49] V. Ramakrishnan and B. F. Feeny, *ASME 2011 Conference DETC2011-48219* (ASME, New York, 2012), p. 761.
- [50] S. Paul and D. S. Ray, [Philos. Trans. R. Soc. A **379**, 20200231 \(2021\)](#).
- [51] R. W. Boyd, *Nonlinear Optics* (Academic Press, Cambridge, UK, 2008).
- [52] C. Santori and Y. Yamamoto, [Nat. Phys. **5**, 173 \(2009\)](#).